



ELSEVIER

Available online at www.sciencedirect.com**ScienceDirect**journal homepage: www.elsevier.com/locate/he

A DFT study of dopant (Zr, Nb) and vacancies on the dehydrogenation on MgH₂ (001) surface



CrossMark

Estefanía Germán^a, Carla Luna^a, Jorge Marchetti^b, Paula Jasen^a, Carlos Macchi^c, Alfredo Juan^{a,*}

^a Instituto de Física del Sur (IFISUR, UNS-CONICET) and Departamento de Física, Universidad Nacional del Sur, Av. Alem 1253, B8000CPB Bahía Blanca, Argentina

^b Department of Mathematical Science and Technology, Norwegian University of Life Sciences, Drøbakveien 31, Ås 1432, Norway

^c IFIMAT, UE CIFICEN (CONICET-UNCPBA), Pinto 399, B7000GHG Tandil, Argentina

ARTICLE INFO

Article history:

Received 24 August 2013

Received in revised form

9 November 2013

Accepted 12 November 2013

Available online 15 December 2013

Keywords:

Magnesium hydride

Surface

DFT

Dehydrogenation

Vacancies

Defects

ABSTRACT

Ab initio calculations were used to study dehydrogenation energy in a set of systems, pure, Nb- or Zr-doped, free of defects and containing vacancy-like defects MgH₂ (001) surface. The preferential location site for dopants was determined by means of occupation energy analysis. Zr atom prefers substitutional and interstitial sites while Nb locates on interstitial site close to the surface. The effect of vacancies in the geometric structure and in dehydrogenation energy was considered. It was found that MgH₂ containing a Mg vacancy doped with Zr, in an interstitial site and the same system containing Mg–H complex vacancy, modify the surface geometry and weakens the Mg–H bonds making easier the dehydrogenation process. When the surface is doped with Nb despite any vacancy generation, the dehydrogenation is less probable energetically in comparison with Zr-doped.

Copyright © 2013, Hydrogen Energy Publications, LLC. Published by Elsevier Ltd. All rights reserved.

1. Introduction

Considering the growing world population, the increasing standard of living in developing countries, the limited supply of fossil fuels and its adverse effect on the environment, the need for sustainable and clean energy has never been bigger.

Hydrogen is a promising fuel source that is attractive as an alternative to fossil fuels, it is considered as a possible solution for the automobile industry. This element is an abundant

elementary resource with huge energy capacity [1]. Pure hydrogen does not exist in nature, so it must come from other resources. The fossil fuel combustion products; such as carbon dioxide, nitric and nitrous oxides, sulfur dioxide and hydrocarbons is today at considerably high levels. Hydrogen is an environmentally benign, safe and attractive vector; being the most abundant element in the universe, with a high energy density per unit weight (chemical energy of hydrogen; 142 MJ/kg is at least three times larger than that of other chemical fuels [1]) and water as the major by-product of its combustion.

* Corresponding author. Tel./fax: +54 2914888218.

E-mail address: cujuan@uns.edu.ar (A. Juan).

Recently, solid-state hydrogen storage has received more attention. This methodology is based upon the chemical or physical combination of hydrogen with the materials in question; which are metal/complex hydrides and carbon based structures. Metal hydrides are seen to be a promising, efficient and safe storage media for on-board vehicle applications. A major disadvantage is that store only about 2%–7% hydrogen by weight. Nevertheless, their volumetric storage density is higher than most of other forms of storage [2].

Magnesium hydride (MgH_2) is the parent compound of an important group of hydrogen storage materials and exhibits high gravimetric and volumetric storage density (7.7% and 55 kg/m³, respectively). Although the practical potential of pure MgH_2 is limited by its high thermodynamic stability and slow kinetics, mechanical treatment and chemical alloying have been shown to improve the kinetics and to reduce the desorption temperatures [3]. However, due to the strong interaction between magnesium (Mg) and hydrogen (H), high desorption temperatures ($\sim 300^\circ\text{C}$ at 1 atm) are required. This fact gives rise to an unacceptable cost of energy. Undesirable poor hydrogen desorption kinetics of some metal hydrides have tried to be improved by several methods. The hydrogenation/dehydrogenation thermodynamics can be improved altering the chemical composition and mechanical alloying.

There are several studies theoretical and experimental related to the reduction of Mg hydride stability, experimentally [4–14].

Song et al. [15] have found a decreasing effects of Cu, Ni, Al, Nb and Fe to Ti, in terms of descending effectiveness order, on stability of Mg hydride, via total energy methods. The analysis of density of states (DOS) and charge distribution results proved that the bonds between Mg and H were weakened due to the effects of alloying elements.

Vegge and his co-workers [16] performed calculations on MgTMH_3 (TM = transition metals) hydrides with perovskite structure. The stability of alloyed hydrides tend to decrease from MgSc to MgFe , where Cu and Zn as impurity elements were not seen to produce the same effect.

In addition to studies on bulk MgH_2 , many more have been carried out on surface structures. Mg–H bonds are weaker on surfaces, reducing the high stability of magnesium hydride [17–20].

Wang and Johnson [21] elucidated the catalytic effect of Ti substitutional dopant on H_2 desorption from MgH_2 (110) surfaces using density functional theory (DFT) calculations. In the case of a Ti-doped surface, they identified a concerted mechanism involving H bulk (vacancy-mediated) diffusion to feed H_2 surface desorption, arising from a synchronized diffusion of H atoms around Ti. The kinetic barrier for the Ti-doped surface is reduced and the catalyzed H_2 desorption is mediated by a change in hydrogen coordination number of Ti, altering the associated Ti spin state.

Dai et al. [22] studied the influence of dopants on the dehydrogenation properties of an Al, Ti, Mn, and Ni doped MgH_2 (110) surface by first principles calculations. It was shown that Al prefers to substitute for an Mg atom, whereas Ti, Mn, and Ni prefer to occupy interstitial sites. The dopants followed different mechanisms to improve the dehydrogenation properties of MgH_2 . They also carried out a

first principle study to investigate the dehydrogenation properties of metal-doped MgH_2 (001) surface [23]. Al and Ti prefer to substitute for Mg atoms, whereas Mn and Ni prefer to occupy interstitial sites.

Periodic DFT and nudged elastic Band (NEB) method have been used by Guangxin Wu et al. to investigate the hydrogen desorption on MgH_2 (001) and MgH_2 (110) surfaces as a first step towards understanding the dehydrogenation cycle [24]. A study of reaction barriers for different pathways on MgH_2 (001) and MgH_2 (110) surfaces have also been performed.

Previous works reported that generation of vacancies in doped bulk MgH_2 structure diminishes its stability while Mg–H bonds strength decreases [25,13].

In this work we studied the preferential site of two dopants (Nb and Zr) on the MgH_2 (001) surface. We also considered vacancy-like defects (Mg, H or Mg–H complexes) in order to analyze the influence of dopants and vacancies on the dehydrogenation properties and electronic structure. We also studied the evolution of chemical bond during dehydrogenation through overlap population analysis.

2. Computational method and models

Energetic and electronic calculations have been performed within the frame of the density functional theory (DFT) [26] which was implemented in the Vienna Ab initio Simulation Package (VASP) code [27,28]. The projector augmented wave (PAW) pseudopotential [27,28] was used to account the electron–ion core interaction, using the PW91 functional as the generalized gradient approximation (GGA) [29] for the exchange–correlation term.

The studied MgH_2 surfaces were simulated using a (2×2) slab containing 5 layers of Mg atoms with a 20 Å vacuum in the [001] direction. We checked the dependence of dopant occupation energy with the size of slabs (1×1), (2×2) and (3×3) . This energy value differs 0.12 eV when the calculation is carried out with (1×1) and (2×2) slabs. The energy value difference is even smaller between (2×2) and (3×3) slabs. In order to reach a balance between accuracy and time of calculation a (2×2) slab model was used. We also checked the influence of strain effect, carrying out a full relaxation of the pure and doped systems and compared the total energy between partial and full relaxation. This difference is lower than 2% in the formation energy calculation implying that the influence of strain effects is weak on the atomic positions in the upper-layers. In the calculation, the Brillouin-zone was sampled using a $6 \times 6 \times 1$ Monkhorst–Pack k-point mesh [30]. For the plane-wave basis set a cut-off of 650 eV was used. We relaxed the first three layers of the slab while the bottom two layers were kept fixed to the bulk positions. The total energy convergence and the forces on the atoms were less than 10^{-4} eV and 0.01 eV/Å, respectively. The self-consistent calculations were considered to converge when the difference in the total energy of the crystal between consecutive steps did not exceed 10^{-5} eV. In the same way, the static calculations were considered to converge using the same criterion. To analyze the electronic structure and bonding we have used the concept of density of states (DOS) and the

overlap population (OP) [31–35]. The OP was calculated using ADF code [36]. Similar analysis was reported in Refs. [25,37].

In a previous work we obtained the calculated lattice parameters for the pure perfect MgH₂ cell, which has a tetragonal structure of rutile type (P42/mnm, group No. 136), specified by a lattice parameter a and the c/a ratio: $a = 4.501 \text{ \AA}$, $c/a = 6.674$, and $u = 3.22 \text{ \AA}$. These results are in good agreement with the experimental values [13,38]. The MgH₂ (001) surface is simulated based on these parameters. As mentioned before, TM dopants are added to the surface, therefore we consider three different situations, TM as a substituent atom replacing a superficial Mg atom (Sub), TM located in an interstitial site 1 (called Inter I) and TM located in an interstitial site 2 (called Inter II). Fig. 1 shows the slab, the different dopants location and the generated vacancies. The occupation energy (E_{occ}) is calculated to identify the preference site of the dopants in the surface and the relative stability of the doped system comparing to the pure MgH₂ system, using the following definition:

$$E_{\text{occ}} = E(\text{Mg}_{20-x}\text{TM}_{x+y}\text{H}_{40}) - [E(\text{Mg}_{20}\text{H}_{40}) + (x+y)E(\text{TM}) - xE(\text{Mg})]$$

being ($x = 1, y = 0$) when TM substitute a superficial Mg atom and ($x = 0, y = 1$) when TM is located in an interstitial site.

Three types of vacancies were also generated in these surfaces: Hydrogen vacancy (vH), Magnesium vacancy (vMg) and the complex Hydrogen–Magnesium vacancy (vHMg). In all cases the extracted atoms are first neighbors to the TM. We also calculated the formation energy of vacancies in all systems:

$$E_{\text{vH}} = E(\text{Mg}_{20-x}\text{TM}_{x+y}\text{H}_{40-1}) + 1/2E(\text{H}_2) - E(\text{Mg}_{20-x}\text{TM}_{x+y}\text{H}_{40})$$

$$E_{\text{vMg}} = E(\text{Mg}_{20-x-1}\text{TM}_{x+y}\text{H}_{40}) + E(\text{Mg}) - E(\text{Mg}_{20-x}\text{TM}_{x+y}\text{H}_{40})$$

$$E_{\text{vHMg}} = E(\text{Mg}_{20-x-1}\text{TM}_{x+y}\text{H}_{40-1}) + 1/2E(\text{H}_2) + E(\text{Mg}) - E(\text{Mg}_{20-x}\text{TM}_{x+y}\text{H}_{40})$$

3. Results and discussions

3.1. Energy calculation

Table 1 shows the obtained energies for dopant location and vacancy generation. Zr dopant atom prefers to substitute the Mg atom and Nb dopant atom prefers to occupy the interstitial site I (Inter I) where the energy values are the smallest in each case (1.310 and 1.950 eV, respectively). Both TM placed in interstitial site II (Inter II) are the least likely dopant positions,

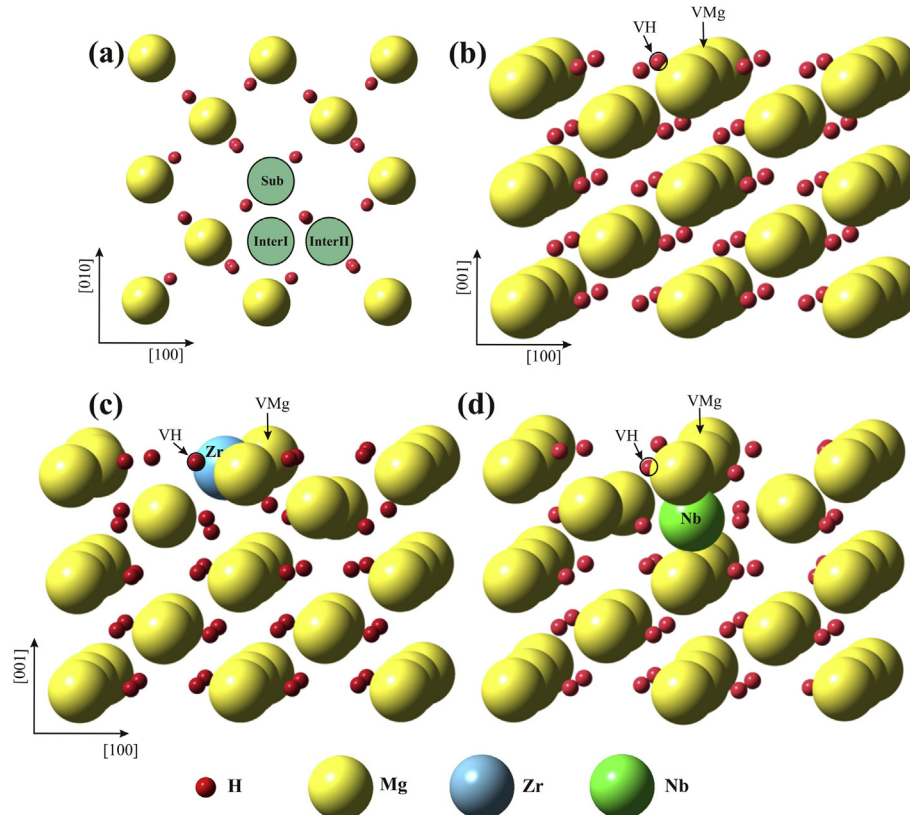


Fig. 1 – (a) Top view of the supercell. The small red and medium yellow balls denote de H and Mg atoms respectively, the medium green circles correspond to substitution and interstitial sites. **(b)** Side view of MgH₂ pure system **(c)** side view of MgH₂Zr (sub) **(d)** side view of MgH₂Nb (Inter I). TM and atoms which are extracted to generate vacancies are shown (vH, vMg and vHMg). (For interpretation of the references to color in this figure legend, the reader is referred to the web version of this article.)

Table 1 – Dopant occupation and vacancy formation energies (in eV) in the MgH₂ (001) surface after geometric relaxation.

	E_{occ}	E_{vH}	E_{vMg}	E_{vHMg}
Pure MgH ₂		1.373	2.490	2.773
MgH ₂ Nb(sub)	2.170	2.903	3.060	3.733
MgH ₂ Nb(InterI)	1.950	2.874	3.500	2.784
MgH ₂ Nb(InterII)	3.630	—	—	—
MgH ₂ Zr(sub)	1.310	2.303	2.260	2.813
MgH ₂ Zr(InterI)	1.880	2.754	1.440	1.743
MgH ₂ Zr(InterII)	4.000	—	—	—

that is the reason why these configurations are not further studied in this work. We also notice from Table 1 that either as substituent or interstitial site I, occupancy energy is lower for Zr dopant compared with the energy for Nb dopant.

The vacancy formation energies (see Table 1), diminish when a Zr dopant atom is added. In the case of a Zr present as Inter I, the favored vacancies are vMg and vHMg, while vMg is preferred when Zr is substitutional. Nb dopant atom does not follow this behavior, the vacancy energy generation increases compared to pure MgH₂.

3.2. Density of states

The total and partial densities of states (DOSS) of the pure MgH₂ (001) surface are shown in Fig. 2 from (b) to (d). The DOS curve corresponding to MgH₂ bulk is also plotted as reference (Fig. 2(a)). In this curve we can see a band gap of approximately 4 eV with a large dispersion of the bands showing the s-like character. The underestimation of the energy gap compared

to experimental findings is expected for this type of calculation [39]. In the case of MgH₂ (001) surface this gap between conduction and valence bands is reduced about 1 eV, the curve above the Fermi level is less intense [23] and DOS curve shows a wide band gap semiconductor behavior. The Fermi level is placed immediately above the valence band and this band spreads out in the energy range from -6.5 eV to the Fermi level and presents a sharp peak at -1 eV. Analyzing the partial DOS we can notice that this correspond to the bonding between Mg and H resulting in a strong hybridization which is responsible for the high formation energy of MgH₂. The conduction band is dominated by Mg s and p states and the valence band mainly by H-s states. In the projected DOS curve for the H atom the intensity is due to the weight of H in the structure and also by the transfer of electron density from Mg to H leading to an ionic hydride. The relative large band gap of MgH₂ leads to a relatively high formation energy of MgH₂ and a poor hydrogen sorption kinetics [40]. The interaction between Mg and H atoms is stronger in bulk than those in the surface, the intensity of the valence band diminishes. These weak Mg–H bonding interactions in the surface make this system more feasible to react with dopants.

The MgH₂Zr-doped (sub) DOS curves are shown in Fig. 2 from (e) to (h). A 2 eV reduction in the band gap is observed. New bands appear above and below the valence band and around E_F there are two sharp peaks, although they are originated from H, Mg and Zr interactions, Zr dopant is the main contributor. The projected DOS curves of Mg and H atoms are reduced at the E_F due to the presence of Zr dopant and the sharp peak now at -3.5 eV diminishes its intensity, decreasing the Mg–H hybridization. These behaviors are attributed to a weakening of Mg–H interaction [41].

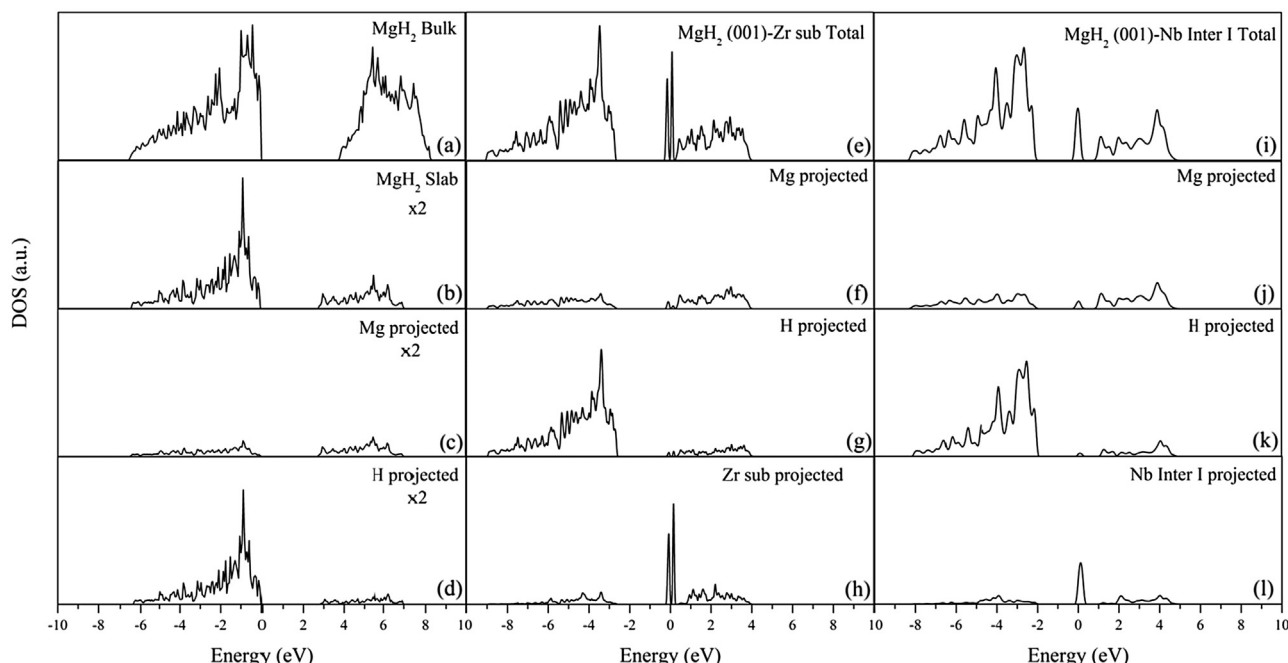


Fig. 2 – Density of states (DOS) curves corresponding to (a) MgH₂ bulk, (b) MgH₂ (001) slab, (c) Mg atoms projected and (d) H atoms projected of MgH₂ surface. (e) MgH₂Zr (sub) total, (f) Mg atoms projected, (g) H atoms projected and (h) Zr atom projected corresponding to MgH₂Zr (sub) surface. (i) MgH₂Nb (Inter I) total, (j) Mg atoms projected, (k) H atoms projected and (l) Nb atom projected corresponding to MgH₂Nb (Inter I) surface.

Table 2 – Dehydrogenation energy, E_{des} (eV), for TM doped and pure MgH_2 (001) surface, with and without vacancies.

	E_{des} (eV)		
	vH	vMg	vHMg
Pure MgH_2	1.376	1.908	2.793
$\text{MgH}_2\text{Nb}(\text{sub})$	0.725	1.436	1.453
$\text{MgH}_2\text{Nb}(\text{InterI})$	0.888	0.810	1.248
$\text{MgH}_2\text{Zr}(\text{sub})$	0.786	1.683	0.815
$\text{MgH}_2\text{Zr}(\text{InterI})$	0.962	1.748	-0.451
			-0.204

The MgH_2 containing Nb (Inter I) and its projected curves are plotted in Fig. 2(i)–(l). Compared to Zr, we detected a reduction in the band gap (~ 1.7 eV) and a sharp peak near the E_F mainly from Nb d orbital, and to a lesser extent to Mg and H orbitals. As in the case of Zr a sharp peak – now at -2.5 eV – diminishes its intensity, decreasing Mg–H hybridization. Previous calculation supports this interpretation [7,22,23,42,43].

Doping leads to the appearance of a narrow d-band in the middle of the band gap with the Fermi level within. Zr atoms have 2 d electrons and Nb atoms have 4 d electrons, as the d-band fills E_F shifts. These d-states are strongly hybridized with s-states of H atoms and form a strong TM-H bonding and decrease the band gaps. We can predict that Mg–H dissociation will be easier and the desorption energy of H will be lower when MgH_2 (001) surface is doped with Zr and Nb atoms.

3.3. Dehydrogenation energies

In order to clarify the effect of dopants and vacancies in the MgH_2 (001) surface, we studied the dehydrogenation energy in the different systems following this definition:

$$E_{des} = E(\text{Mg}_{20-x}\text{M}_{x+y}\text{H}_{40-1}) + 1/2E(\text{H}_2) - E(\text{Mg}_{20-x}\text{M}_{x+y}\text{H}_{40})$$

where $\text{Mg}_{20-x}\text{M}_{x+y}\text{H}_{40-1}$ is a pseudo-structure in which a H atom is taken away from the relaxed $\text{Mg}_{20-x}\text{M}_{x+y}\text{H}_{40}$ system. The energy of molecular hydrogen is estimated as -6.77 eV using a $10 \times 10 \times 10$ Å supercell [22]. We extracted a superficial H atom near the defects. The dehydrogenation values for the different cases are listed in Table 2.

In the literature, it was reported that the theoretical MgH_2 dehydrogenation energy for the bulk is 1.60 eV while the experimental value is 1.70 eV [44,45]. This energy in the case of

pure MgH_2 (001) surface the energy is lower because Mg–H bonds are not as strong as in the bulk. The overlap population values (see Section 3.4) for Mg–H bonds, in the surface are about 0.400, while in the bulk are 0.595 [25].

This dehydrogenation energy decrease considerably in doped systems (from 30% to 47%), being more notorious when the dopant is located in the substitutional place. After relaxation, the superficial Mg–H bonds are lengthened approximately 10% compared to the pure solid, in this way it is easier to break these bonds and release one H atom. In the case of substitutional locations the dopant moves from its original position towards the center of the surface, as well as in the interstitial locations the dopant atom does not move significantly, however the neighboring atoms change their positions considerably, weakening the Mg–H bonds.

On the other hand, the dehydrogenation energy increases in the pure MgH_2 when vacancies are generated. Except for $\text{MgH}_2\text{Nb}(\text{sub})$ -vMg, when vacancies are present in the doped systems the dehydrogenation energy decreases in comparison with the pure MgH_2 (001) containing the same vacancies.

Table 2 presents two negative values for dehydrogenation energy, $\text{MgH}_2\text{Zr}(\text{InterI})$ -vMg and $\text{MgH}_2\text{Zr}(\text{InterI})$ -vHMg. This implies that a spontaneous dehydrogenation of H atom could be expected in these systems. The relaxed geometry for these two configurations favors the hydrogen desorption weakening Mg–H bonds and decreasing the number of H bonds, allowing its extraction without requiring a high energy cost. Notice that the vacancy formation energies for these systems are the lowest (see Table 1). In Fig. 3 the geometries of (a) $\text{MgH}_2\text{Zr}(\text{InterI})$, (b) $\text{MgH}_2\text{Zr}(\text{InterI})$ -vMg and (c) $\text{MgH}_2\text{Zr}(\text{InterI})$ -vHMg are displayed. When a vMg is generated, the Zr atom moves towards the empty space that vMg left in the structure, this action causes an upward displacement of a surface H atom. After dehydrogenation, the atoms rearrange in the structure with a more stable configuration.

3.4. Overlap population analysis

Table 3 presents the OP values for bonds in different systems, the number beside each element indicates the layer in which it is located. In the case of MgH_2 (001) surface Mg–Mg bonds are about 91% weaker than Mg–H bonds and we can notice that the generation of vacancies (vH and vMg) produces a decrease in the Mg–H OP values, between 3% and 6% depending on the H atom position, first or second layer. In the case of complex vacancy (vHMg) generation, the Mg–Mg bond

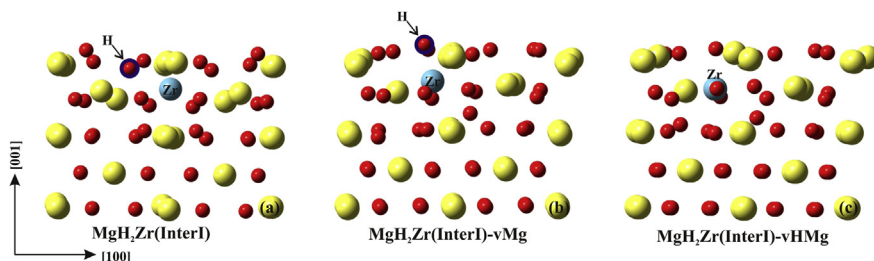


Fig. 3 – (a) $\text{MgH}_2\text{Zr}(\text{InterI})$, (b) $\text{MgH}_2\text{Zr}(\text{InterI})$ -vMg, (c) $\text{MgH}_2\text{Zr}(\text{InterI})$ -vHMg atom positions after relaxation. The hydrogen atom lost during dehydrogenation process is identified with a blue circle. (For interpretation of the references to color in this figure legend, the reader is referred to the web version of this article.)

Table 3 – Overlap population (OP) values. The number beside each element denotes the layer in which it is placed.

Overlap population				
Bond	Defect			
	Pure	vH	vMg	
System MgH ₂				
Mg–Mg ₂	0.024	0.024	0.028	0.019
Mg–Mg ₃	0.032	0.030	0.030	0.023
Mg–H1	0.427	0.429	0.401	0.367
Mg–H2	0.277	0.268	0.263	0.271
System MgH ₂ Nb (sub)				
Mg–Mg	0.000	0.000	0.000	0.000
	0.031	0.024	0.000	0.000
Mg–H1	0.249	0.232	0.000	0.183
Mg–H2	0.286	0.283	0.164	0.159
TM1–H1	0.382	0.406	0.427	0.449
TM1–H2	0.417	0.382	0.425	0.464
TM–Mg	0.074	0.063	0.000	0.149
System MgH ₂ Nb (Inter I)				
Mg–Mg	0.038	0.000	0.039	0.008
	0.009	0.011	0.123	0.000
Mg–H1	0.170	0.161	0.158	0.164
Mg–H2	0.112	0.125	0.091	0.099
TM2–H2	0.438	0.441	0.445	0.439
TM2–H1	0.413	0.409	0.431	0.406
TM2–Mg	0.171	0.154	0.134	0.115
System MgH ₂ Zr (sub)				
Mg–Mg	0.028	0.017	0.023	0.019
	0.033	0.035	0.028	0.028
Mg–H1	0.406	0.413	0.315	0.329
Mg–H2	0.247	0.217	0.299	0.332
TM–H	0.000	0.000	0.000	0.000
	0.235	0.231	0.255	0.224
TM–Mg	0.000	0.000	0.000	0.000
System MgH ₂ Zr (Inter I)				
Mg–Mg	0.049	0.037	0.029	0.027
	0.023	0.039	0.041	0.031
Mg–H1	0.106	0.221	0.196	0.299
Mg–H2	0.088	0.083	0.233	0.252
TM–H	0.167	0.184	0.207	0.227
	0.235	0.218	0.206	0.165
TM–Mg	0.159	0.070	0.027	0.021

MgH₂ bulk: Mg–Mg bond OP: 0.005; Mg–H bond OP: 0.595, according to C. Luna et al. [25].

OP value diminishes 28% (from 0.032 to 0.023) and Mg–H1 14% (from 0.427 to 0.367).

When the pure system is doped with a Nb atom, the desorption energy values are 0.888 and 0.725 eV for Nb interstitial and substitutional respectively (see Table 2), however the occupation energy is higher when Nb replace a Mg atom, this indicates that MgH₂Nb (sub) system is energetically less probable to occur. We can observe in Table 3 that in MgH₂Nb (sub) the Mg–Mg bonds practically disappear, Mg–H1 bonds get 42% weaker in comparison with MgH₂ pure system, when Nb atom is located in an interstitial place Mg–H bond strength decrease approximately 60% in relation to the undoped system. Nb–H bond OP values in both cases are similar (about 0.400), a strong orbital overlapping is present between these

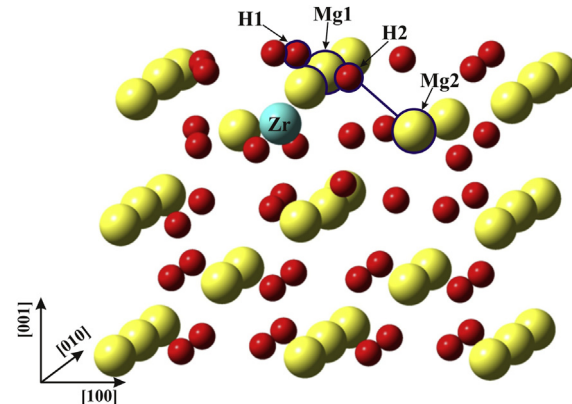


Fig. 4 – Mg–H bonds which increase their strength in MgH₂Zr(InterI)-vMg after dehydrogenation.

atoms. When defects are present, Mg–H bond diminishes its strength, Nb–H bonds maintain their high OP value, observing the final configurations it seems to be the beginning of a beta-NbH structure formation [46–49]. In both cases, system doped with Nb atoms, the calculated OP values between TM and neighbor H increase when vacancy-type defects are present, being more notorious for MgH₂Nb (sub).

When the system is doped with Zr atom, we can notice from Table 3 a weakening in Mg–H bonds being more significant for MgH₂Zr (Inter I), 75% in the case of Mg–H1 bonds and 68% for Mg–H2. Zr–H bonds appear (OP values around 0.200), due to the formation of a new ZrH hydride system [50–52].

Relaxed doped systems containing vacancies rearrange their geometry leaving some H atoms exposed above the surface plane. This configuration favors the hydrogen desorption. According to dehydrogenation energies, this reaction is more likely to occur in MgH₂Zr (InterI)-vMg system. In Table 3 we can see that after desorption of H the Mg–H bonds become stronger from 0.196 to 0.299 and from 0.233 to 0.252 (Mg1–H1 and Mg2–H2 in Fig. 4 respectively) demonstrating that the new configuration is more stable. Hydrogen atoms also are bonded to the TM, in Table 3 some OP values for these bonds are shown. When the system is doped with Zr the strength of TM–H bond is weaker than the same system doped with Nb. When Zr atom is placed in an interstitial site (Inter I) this weakening is more noticeable as we generate vacancies in the system.

4. Conclusions

First principles calculations were performed to study the MgH₂ (001) surface doped with Nb or Zr. We also analyzed the effect of generating vacancies in the dehydrogenation energy. Zr dopant atom prefers to substitute the Mg atom and Nb dopant atom prefers to occupy the interstitial site I (Inter I). The occupancy energy is lower for Zr dopant compared with the energy for Nb dopant. Based on the DOS study we found that the decrease in band gaps and bond strengths lead to an easier Mg–H dissociation and lower desorption energy of H when MgH₂ (001) surface is doped

with these TM. This dehydrogenation energy decrease considerably in doped systems and the neighboring atoms change their positions noticeably, weakening the hydrogen bonds. By calculating dehydrogenation energy, it was found that MgH₂Zr(Interstitial)-vMg and MgH₂Zr(Interstitial)-vHMg systems desorb H spontaneously, not requiring any energy cost. The dopants and vacancies generation, alter the geometry of the surface, reducing its stability. We can conclude that Zr-doped improves the dehydrogenation energy better than Nb doped, and that the generation of vacancies helps to lower this energy. In this way, Zr placed in the interstitial site 1 containing a vacancy of Mg is the best combination to obtain a lower desorption energy.

Acknowledgements

The authors acknowledge SGCyT (UNS), IFISUR-CONICET, CIFICEN (CIC-UNICEN-CONICET), PICT 1770, 1609 and CIC Provincia de Buenos Aires for financial support. All authors are members of CONICET.

REFERENCES

- [1] Schlapbach L, Zuttel A. Hydrogen-storage materials for mobile applications. *Nature* 2001;414:353–8.
- [2] Perruzini M, Poli R. Recent advances in hydride chemistry. In: *Hydrides for hydrogen storage*, 18; 2001. p. 531.
- [3] Sakintuna B, Lamari-Darkrim F, Hirscher M. Metal hydride materials for solid hydrogen storage: a review. *Int J Hydrogen Energy* 2007;32:1121–40.
- [4] Xie L, Liu Y, Zhang X, Qu J, Wang Y, Li X. Catalytic effect of Ni nanoparticles on the desorption kinetics of MgH₂ nanoparticles. *J Alloy Compd* 2009;482:388–92.
- [5] Shang CX, Bououdina M, Song Y, Guo ZX. Mechanical alloying and electronic simulations of (MgH₂ + M) systems (M = Al, Ti, Fe, Ni, Cu and Nb) for hydrogen storage. *Int J Hydrogen Energy* 2004;29:73–80.
- [6] Jensen TR, Andreasen A, Vegge T, Andreasen JW, Ståhl K, Pedersen AS, et al. Dehydrogenation kinetics of pure and nickel-doped magnesium hydride investigated by in situ time-resolved powder X-ray diffraction. *Int J Hydrogen Energy* 2006;31:2052–62.
- [7] Yu XB, Yang ZX, Liu HK, Grant DM, Walker GS. The effect of a Ti-V-based BCC alloy as a catalyst on the hydrogen storage properties of MgH₂. *Int J Hydrogen Energy* 2010;35:6338–44.
- [8] Janot R, Darok X, Rougier A, Aymard L, Nazri GA, Tarascon JM. Hydrogen sorption properties for surface treated MgH₂ and Mg₂Ni alloys. *J Alloy Compd* 2005;404–406:293–6.
- [9] Checchetto R, Bazzanella N, Miotello A, Mengucci P. Catalytic properties on the hydrogen desorption process of metallic additives dispersed in the MgH₂ matrix. *J Alloy Compd* 2007;446–447:58–62.
- [10] Bazzanella N, Checchetto R, Miotello A. Atoms and nanoparticles of transition metals as catalysts for hydrogen desorption from magnesium hydride. *J Nanomater*;2011. 11 pp. [Article ID 865969]. <http://dx.doi.org/10.1155/2011/865969>.
- [11] Hanada N, Ichikawa T, Fujii H. Catalytic effect of nanoparticle 3d-transition metals on hydrogen storage properties in magnesium hydride MgH₂ prepared by mechanical milling. *J Phys Chem B* 2005;109:7188–94.
- [12] Tsuda M, Diño WA, Kasai H, Nakanishi H, Aikawa H. Mg–H dissociation of magnesium hydride MgH₂ catalyzed by 3d transition metals. *Thin Solid Films* 2006;509:157–9.
- [13] Luna CR, Germán E, Macchi C, Juan A, Somoza A. On the perfect MgH₂(–Nb, –Zr) systems and the influence of vacancy-like defects on their structural properties. A self-consistent first principle calculations study of the electron and positron parameters. *J Alloy Compd* 2013;556:188–97.
- [14] Chen D, Wang YM, Chen L, Liu S, Ma CX, Wang LB. Alloying effects of transition metals on chemical bonding in magnesium hydride MgH₂. *Acta Mater* 2004;52:521–8.
- [15] Song Y, Guo ZX, Yang R. Influence of selected alloying elements on the stability of magnesium dihydride for hydrogen storage applications: a first-principles investigation. *Phys Rev B Condens Matter* 2004;69:094205–16.
- [16] Vegge T, Hedegaard-Jensen LS, Bonde J, Munter TR, Nørskov JK. Trends in hydride formation energies for magnesium-3d transition metal alloys. *J Alloy Compd* 2005;386:1–7.
- [17] Hussain T, De Sarkar A, Adit Maark T, Sun W, Ahuja R. Strain and doping effects on the energetics of hydrogen desorption from the MgH₂ (001) surface. *EPL J* 2013;101. 27006-p1–p6.
- [18] Fedorov AS, Serzhantova MV, Kuzubov AA. Analysis of hydrogen adsorption in the bulk and on the surface of magnesium nanoparticles. *J Exp Theor Phys* 2008;107:126–32.
- [19] Du AJ, Smith SC, Yao XD, Lu GQ. The role of Ti as a catalyst for the dissociation of hydrogen on a Mg(0001) surface. *J Phys Chem B* 2005;109:18037–41.
- [20] Du AJ, Smith SC, Yao XD, Lu GQ. First-principle study of adsorption of hydrogen on Ti-doped Mg(0001) surface. *J Phys Chem B* 2006;110:21747–50.
- [21] Wang LL, Johnson DD. Hydrogen desorption from Ti-doped MgH₂(110) surfaces: catalytic effect on reaction pathways and kinetic barriers. *J Phys Chem C* 2012;116:7874–8.
- [22] Dai JH, Song Y, Yang R. First principles study on hydrogen desorption from a metal (=Al, Ti, Mn, Ni) doped MgH₂ (110) surface. *J Phys Chem C* 2010;114:11328–34.
- [23] Dai JH, Song Y, Yang R. Intrinsic mechanisms on enhancement of hydrogen desorption from MgH₂ by (001) surface doping. *Int J Hydrogen Energy* 2011;36:12939–49.
- [24] Wu G, Zhang J, Li Q, Wu Y, Chou K, Bao X. Dehydrogenation kinetics of magnesium hydride investigated by DFT and experiment. *Comput Mater Sci* 2010;49:S144–9.
- [25] Luna CR, Macchi CE, Juan A, Somoza A. Electronic and bonding properties of MgH₂–Nb containing vacancies. *Int J Hydrogen Energy* 2010;35:12421–7.
- [26] Kohn W, Sham LJ. Self-consistent equations including exchange and correlation effects. *Phys Rev* 1965;140:A1133–1138.
- [27] Kresse G, Joubert D. From ultrasoft pseudopotentials to the projector augmented-wave method. *Phys Rev B* 1999;59:1758–75.
- [28] Blöchl PE. Projector augmented-wave method. *Phys Rev B* 1994;50:17953–79.
- [29] Perdew JP, Wang Y. Accurate and simple analytic representation of the electron-gas correlation energy. *Phys Rev B* 1992;45:13244–9.
- [30] Monkhorst HJ, Pack JD. Special points for Brillouin-zone integrations. *Phys Rev B* 1976;13:5188–92.
- [31] Baerends EJ, Ellis DE, Ros P. Self-consistent molecular Hartree-Fock-Slater calculations I. The computational procedure. *Chem Phys* 1973;2:41–51.
- [32] te Velde G, Baerends EJ. Numerical integration for polyatomic systems. *J Comp Phys* 1992;99:84–98.
- [33] Fonseca Guerra C, Visser O, Snijders JG, te Velde G, Baerends EJ. METE CC-1995;95:305.
- [34] Hohenberg P, Kohn W. Inhomogeneous electron gas. *Phys Rev* 1964;136:B864–71.

- [35] Hoffmann R. Solids and surfaces: a chemist's view of bonding in extended structures. New York: VCH; 1988.
- [36] ADF 2.2.1. Theoretical chemistry. Amsterdam: Vrije Universiteit; 1997.
- [37] López-Corral I, Germán E, Juan A, Volpe MA, Brizuela GP. Hydrogen adsorption on palladium dimer decorated graphene: a bonding study. *Int J Hydrogen Energy* 2012;37:6653–65.
- [38] Bortz M, Bertheville B, Böttger G, Yvon K. Structure of the high pressure phase γ -MgH₂ by neutron powder diffraction. *J Alloy Compd* 1999;287:L4–6.
- [39] Yu R, Lam PK. Electronic and structural properties of MgH₂. *Phys Rev B* 1988;37:8730–7.
- [40] Zeng XQ, Cheng LF, Zou JX, Ding WJ, Tian HY, Buckley C. Influence of 3d transition metals on the stability and electronic structure of MgH₂. *J Appl Phys* 2012;111:093720–9.
- [41] Shelyapina MG, Fruchart D. Role of transition elements in stability of magnesium hydride: a review of theoretical studies. *Diffus Defect Data B Solid State Phenom* 2011;170:227–31.
- [42] Li S, Jena P, Ahuja R. Dehydrogenation mechanism in catalyst-activated MgH₂. *Phys Rev B* 2006;74:132106–10.
- [43] Maark TA, Hussain T, Ahuja R. Structural, electronic and thermodynamic properties of Al- and Si-doped α -, γ -, and β -MgH₂: density functional and hybrid density functional calculations. *Int J Hydrogen Energy* 2012;37:9112–22.
- [44] Kresse G, Hafner J. Ab initio molecular-dynamics for liquid metals. *Phys Rev B* 1993;47:558–61.
- [45] Fernandez JF, Sanchez CR. Simultaneous TDS-DSC measurements in magnesium hydride. *J Alloy Compd* 2003;356–357:348–52.
- [46] Tao HJ, Ho KM, Zhu XY. Investigation of the electronic structure and phonon anharmonicity in β - and γ -NbH. *Phys Rev B Condens Matter* 1986;34(12):8394–400.
- [47] Birnbaum HK, Grossbeck ML, Amano M. Hydride precipitation in Nb and some properties of NbH. *J Less-Common Met* 1976;49:357–70.
- [48] Hauck J. Structural relations between vanadium, niobium, tantalum hydrides and deuterides. *Acta Crystallogr* 1978;A34:389–99.
- [49] Hauck J. Ordering of hydrogen in niobium hydride phases. *Acta Crystallogr* 1977;A33:208–11.
- [50] Gulbransen EA, Andrew KF. Crystal structure and thermodynamic studies on the zirconium-hydrogen alloys. *J Electrochem Soc* 1954;101:474–80.
- [51] Weaver JH, Peterman DJ, Peterson DT, Franciosi A. Electronic structure of metal hydrides. IV. TiH_x, ZrH_x, HfH_x, and the fcc-fct lattice distortion. *Phys Rev B* 1981;23(4):1692–8.
- [52] Couch JG, Harling OK, Clune LC. Structure in the neutron scattering spectra of zirconium hydride. *Phys Rev B* 1971;4:2675–81.